



Balancing autonomy and utilization of solar power and battery storage for demand based microgrids



Matthew T. Lawder ^a, Vilayanur Viswanathan ^b, Venkat R. Subramanian ^{a, c, *}

^a Energy, Environmental, and Chemical Engineering Department, Washington University in St. Louis, 1 Brookings Dr., St. Louis, MO 63130, USA

^b Pacific Northwest National Laboratory, 902 Battelle Blvd., Richland, WA 99354, USA

^c Department of Chemical Engineering, University of Washington, Box 351750, Seattle, WA 98195, USA

HIGHLIGHTS

- Microgrids with solar power and energy storage are studied through modeling.
- A single particle battery model was used to study microgrid battery storage.
- System demand effects for microgrids are examined.
- Results on microgrid autonomy and battery usage are report for differing demands.
- Seasonal solar variation reduces battery utilization from optimal levels.

ARTICLE INFO

Article history:

Received 22 August 2014

Received in revised form

18 December 2014

Accepted 4 January 2015

Available online 6 January 2015

Keywords:

Microgrid

Battery utilization

Optimal sizing

Autonomy

Solar integration

Single particle model

ABSTRACT

The growth of intermittent solar power has developed a need for energy storage systems in order to decouple generation and supply of energy. Microgrid (MG) systems comprising of solar arrays with battery energy storage studied in this paper desire high levels of autonomy, seeking to meet desired demand at all times. Large energy storage capacity is required for high levels of autonomy, but much of this expensive capacity goes unused for a majority of the year due to seasonal fluctuations of solar generation. In this paper, a model-based study of MGs comprised of solar generation and battery storage shows the relationship between system autonomy and battery utilization applied to multiple demand cases using a single particle battery model (SPM). The SPM allows for more accurate state-of-charge and utilization estimation of the battery than previous studies of renewably powered systems that have used empirical models. The increased accuracy of battery state estimation produces a better assessment of system performance. Battery utilization will depend on the amount of variation in solar insolation as well as the type of demand required by the MG. Consumers must balance autonomy and desired battery utilization of a system within the needs of their grid.

© 2015 Elsevier B.V. All rights reserved.

1. Introduction

In the past decade, distributed energy resources (DER) have seen rapid growth as more small scale technologies for power generation have become economically favorable. DER growth has driven more communities and individual entities to operate Microgrids (MG), which allow consumers greater control over their energy resources [1]. Many of the DERs that are present in MGs are intermittent, renewable based generation such as solar and wind power.

In order to be used effectively, these systems must utilize energy storage to provide power during times when generation is not producing at full capacity.

Within the electric grid, power generation must match consumer demand in real-time. Since electricity is perishable (it must be used immediately upon creation) and consumer demand can fluctuate on a short (seconds and minutes) timescale, power generation is often run in excess of actual demand requirements in order to maintain the minimum level of electricity required by the grid [2,3]. Energy storage can help to remove the perishable nature of electricity [4]. Energy storage is already used within the electric grid in the form of flywheels and other short term storage methods (used for spinning reserve) which help alleviate some of the excess

* Corresponding author. Department of Chemical Engineering, University of Washington, Box 351750, Seattle, WA 98195, USA.

E-mail addresses: mtlawder@wustl.edu (M.T. Lawder), Vilayanur.viswanathan@pnl.gov (V. Viswanathan), vsubram@uw.edu (V.R. Subramanian).

capacity requirements, maintaining a robust and flexible grid. This type of storage however has a very short discharge time, and due to friction and kinetic losses will lose most of its stored energy within 15 min [5]. Applications where energy storage is useful in the current electric grid and MGs include: system regulation (frequency and voltage), spinning reserve, peak shaving, peak shifting, load leveling, and transmission support [6,7].

MGs combine DER and energy storage, allowing consumers to set up local electrical networks where power is produced and consumed without being transmitted over long distances. Two types of MGs exist: islanded and grid-tied systems. Islanded systems are not connected to any regional or national grids and must generate all of their power within the MG [8]. Grid tied systems can operate in islanded modes (sometimes referred to as emergency mode), however, they maintain a connection to the grid and will typically draw power from the grid during times of high demand and low internal generation. They will send power to the grid during times of high internal generation and low demand [9]. A grid-tied system will only go into islanded mode when the external grid has a failure and cannot supply power to the MG [10]. Grid-tied systems are less strict in their requirements for generation and storage sources because they can use the grid to supplement any power shortfalls and will take energy directly from the grid when economically favorable.

When deciding the desired autonomy of the system (the amount of time that the MG output will match demand), islanded systems will need to operate near 100% autonomy to be effective, while grid-tied systems can operate at lower levels [11]. Autonomy is the inverse metric of Loss of Power Supply Probability (LPSP) used in similar studies [12]. The desire for 100% autonomy can lead systems to be overbuilt (only using their theoretical capacity a few days per year) [13]. This paper studies how to maximize capacity usage based on a combination of demand and generation requirements.

Sizing and system performance analyses of battery systems have been performed for grid applications in connection with conventional generation sources [14], single intermittent renewable sources [15–17] and combined hybrid renewable source systems [11,12,18–20]. Inclusion of system demand within MGs has increased the fidelity of simulations [21]. However, when accounting for battery systems, these simulations utilize simple empirical-based or equivalent-circuit based models (ECM). When sizing and analyzing system performance for battery storage within grid applications, accurate measurements of state-of-charge (SOC) are required for both controlling the battery and monitoring the depth-of-discharge (DOD). The previous work mentioned above has not utilized models rigorous enough to provide accurate measurements of battery utilization and SOC throughout long simulation periods. Using inaccurate models for battery systems forces underutilization of battery capacities in order to maintain safe and continuous operation. Previous work has restricted the operational SOC range and limited DOD during operation [22]. Additionally, empirically based models struggle to account for capacity fade and changes to operating conditions. We show that using the SPM, autonomy and battery utilization can be tracked accurately over the course of an entire year, avoiding the problem of refitting the ECM for changing seasonal insolation.

1.1. Common definitions

The following terms and metrics will be used in assessing the system operational characteristics.

- **State-of-Charge (SOC):** The percentage of a full charge that remains stored in the battery. A fully charged battery will have a SOC

of 100% and a completely discharged battery will have a SOC of 0%. Our studies use lithium anode concentration to track SOC:

$$SOC = \frac{C_n^s}{C_{\max,n}^s} \quad (1.1)$$

- **Depth-of-Discharge (DOD):** The percentage of capacity used during a discharge cycle. We track DOD based on SOC:

$$DOD = SOC_{\text{initial}} - SOC_{\text{final}} \quad (1.2)$$

- **Battery Utilization:** The amount of storage capacity used during battery storage. If a battery experiences a full discharge during one daily cycle, the battery utilization will be 100%. To track this metric in the SPM, all discharge energy is summed and divided by the energy discharged during a single 100% DOD discharge. For systems that experience a single cycle per day, this term approximates to the average DOD for a battery. For real systems this value could be greater than one if multiple deep cycles are experienced on a daily basis.

$$\text{Battery Utilization}_{\text{Annual}} = \frac{\sum \text{Energy}_{\text{discharged}}}{365(\text{Energy}_{100\%DOD})} \quad (1.3)$$

- **Maximum Power Demand to Maximum Solar Power Output Ratio (MDMP):** This metric measures how the power demand relates to the power output from the solar array. For a solar array that has a maximum power rating of 1 MW, a MDMP ratio equal to one would correspond to a maximum power demand of 1 MW. The amount of energy that is demanded will vary based on the shape of the demand curve. The ratio is used so that the demand can be studied independently of the solar array and battery size.
- **Battery Energy Capacity to Solar Energy Capacity Ratio (BCSC):** This metric measures the energy storage capacity of the battery in relation to the amount of energy supplied from the solar array during a day of 12 h solar insolation with no cloud cover. A ratio of one would mean that all of the energy produced by a solar array during a 12 h day could be stored in the battery. The BCSC ratio accounts for the energy capacity of the battery storage system. For most studies that BCSC will remain constant because the size of the solar array and battery capacity will remain constant, while different levels of demand are studied by altering the MDMP ratio (increasing the MDMP will simulate a larger demand for the same sized system).

This paper has defined the MDMP and BCSC ratios as new terms which help the analysis of combined solar-battery systems by allowing comparison between systems, independent of a specific system (or demand) size.

2. Microgrid elements

Three important elements of the MG model are: demand, generation, and storage. The relationship between these three

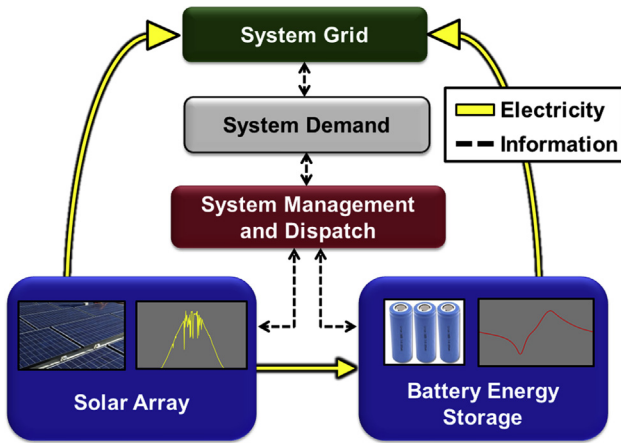


Fig. 1. Schematic showing how information and energy is transferred throughout the MG.

elements within the MG is shown pictorially in Fig. 1. More on the connection between these components is discussed in the following subsections.

2.1. MG demand


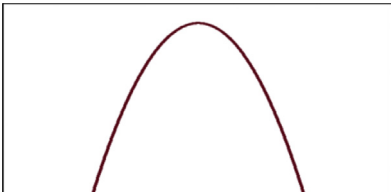

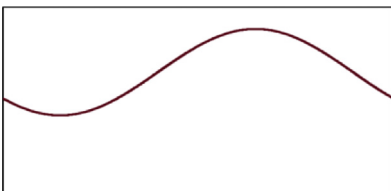
Each MG will have a load profile for the power it needs to operate. These loads will vary over the course of a day and can

change seasonally. Grid-tied MGs have to determine what portions of their demand will be covered by the MG's generation instead of being supplied from the external grid. Some MG systems will use energy storage for arbitrage purposes, meaning charge is stored using the electric grid when electric prices are cheap and released to the MG when electric prices are high. This practice focuses on using storage based on the economic variations in the electric market rather than utilizing the available generation most effectively and can cause a MG to demand more energy than required by its immediate loads. In our study, we exclude the application of arbitrage and assume that the MG demand will never exceed its load.

Different demand structures (driven by different application's needs) will create varying needs among energy generation and storage components. Four different types of demands were studied (shown in Table 1): Trapezoidal; Parabolic, Constant; and Sinusoidal. These types of demand are representative of different needs for both islanded and grid-tied systems.

The total size and amount of individual loads that are being powered through a solar and battery MG system affects the discreteness of the demand. For a small number of defined loads the demand can change swiftly depending on when the loads are turned on or off. Individual case studies have looked at discrete loads but have been limited in their scope for being applied generally [23,24]. For systems supporting many loads, the demand curve will show smoother characteristics because the relative change caused by any individual load will become much smaller. For our simulations, we used demand curves that are approximate

Table 1
Demand curves studied.

| Demand type | Duration | Description | Shape |
|-------------|----------|---|---|
| Trapezoid | 4–10 h | One hour of linear rising demand to max power, constant max power, one hour of linear falling demand |  |
| Parabola | 4–10 h | A parabolic shaped curve that reaches max power at its midpoint |  |
| Constant | 24 h | A steady demand curve that remains the same the entire day |  |
| Sinusoid | 24 h | A sine curve with a 24 period (all day) with a minimum of 1/2 max power (amplitude 1/4 max power) occurring at 3:30AM and maximum occurring at 3:30PM |  |

for systems of large enough size to reduce discrete demand fluctuations.

2.2. Power generation

After determining the portion of the MG's demanded power and duration that will need to be supplied internally, the generation source must be sized so that it can produce the daily energy required. For this paper, solar power is the only generation source within the MG considered. Therefore, the amount of energy produced will be dependent on the size of the solar array and the daily insolation characteristic of the MG site. For complete utilization, the total amount of energy demanded from the system should equal the total amount of energy generated by the system:

$$\int_{t_{s,demand}}^{t_{t,demand}} P_D(t)dt = \int_{sunrise}^{sunset} P_G(t)dt \quad (2.1)$$

where P_D is the instantaneous power demanded and P_G is the instantaneous power generated. Average values for daily solar energy insolation data are available for any US location through NREL's SWERA database and will allow for an estimate for how large a system will need to be [25]. The average values do not show how a location's insolation will change seasonally.

2.3. Energy storage

While energy storage creates flexibility for power delivery within a MG, it remains expensive, and therefore only the amount of storage capacity that is required to meet demand should be added. To determine how much storage capacity is needed within a system, the difference between the power generation curve and power demand curve must be ascertained. When generation occurs at the same time as demand, power generated can be sent directly to the MG without energy storage. The remaining difference will have to be stored for later use as shown below:

$$\text{When } P_G > P_D \text{ Then } \int (P_G(t) - P_D(t))dt = \text{Capacity}_{Storage} \quad (2.2)$$

It is assumed that excess energy will not go to any external grid, but will be focused on being used directly within the MG.

For the cases studied in this paper using only solar power for generation, the amount of capacity needed will vary seasonally due to changes to day length and therefore total daily energy will also vary. Additionally, the charging rate will affect the charging efficiency, which can skew the measured capacity [26]. However, we assume near 100% coulombic efficiency for the battery model so that no side reactions occur during cycling. To determine the required capacity, battery utilization (how much of total capacity is used daily) is studied in conjunction with system autonomy. In this study, we assume that the battery can safely undergo 100% DOD without side effects.

3. Solar and battery models

A wide range of models are available for the individual structures present in solar-battery systems [27]. In the case of MG simulations, the models should be both representative of the systems (accurate) and computationally efficient (fast). For solar insolation and power generation from panels, we use perfect half sine curves that are scaled depending on the length of the day. The day length is varied to simulate seasonal changes in solar insolation. These insolation curves are run through a circuit based solar

model that yields a power output which can be fed into the MG [28]. The maximum power output is scaled depending on the study to maintain a set ratio of capacity with the battery model. The I–V curve for the solar array was obtained using the circuit equation:

$$I = I_{PV} - I_0 \left[\exp\left(\frac{V + R_s I}{V_t a}\right) - 1 \right] - \frac{V + R_s I}{R_p} \quad (3.1)$$

where I is the solar array current, I_{PV} is the photovoltaic current, I_0 is the saturation current, V is the solar array voltage, V_t is the thermal voltage, R_s is the series resistance, R_p is the parallel resistance, and a is the diode ideality constant. Because of the static nature of the solar array during simulation, a circuit model approximation for the solar cell is relevant, while the dynamic battery cannot be accurately modeled with a circuit element.

The lithium ion battery system simulated here contains two porous electrodes and a separator with electrolyte in all three regions. For the battery, we use a single particle model (SPM) that approximates the dynamics of a battery's porous electrode with a single particle for each electrode while incorporating battery kinetics [29]. In a discharged state, lithium is typically stored in the cathode as a metal oxide compound. In order for charging to occur, lithium must diffuse to the electrode surface, deintercalate from the cathode, transport through the electrolyte as a lithium ion to the anode surface, and then intercalate into the anode where it can be stored until discharge. Fick's 2nd law governs the diffusion of lithium through the solid electrodes (assuming spherical particles and diffusion as the only mechanism of transport inside the particles) defined as [30]:

$$\frac{\partial c_i^s}{\partial t} = D_{s,i} \left(\frac{\partial^2 c_i^s}{\partial r^2} + \frac{2}{r} \frac{\partial c_i^s}{\partial r} \right) \quad i = n, p \quad (3.2)$$

where c^s is the solid phase lithium concentration, D_s is the diffusion coefficient for the electrode, and i represents either the positive (cathode) or negative (anode) electrode. Here, the electrode is represented as a single particle that contains the surface area representative of the actual electrode [31]. The intercalation/deintercalation reaction is controlled by Butler–Volmer kinetics described as [32]:

$$j_i = 2k_i \left(c_{\max,i}^s - c_i^s \right)^{0.5} c_i^{s0.5} c^{0.5} \sinh \left[\frac{0.5F}{RT} (\Phi_1 - \Phi_2 - U_i) \right] \quad i = n, p \quad (3.3)$$

where j is the flux into the electrode particle, k is the reaction rate constant for intercalation/deintercalation, c_{\max}^s is the maximum solid phase concentration of the electrode, c is the liquid phase lithium ion concentration, F is Faraday's constant, R is the gas constant, T is the temperature, Φ_1 is the solid phase potential, Φ_2 is the liquid phase potential, and U is the open circuit potential. For low to medium charging rates, the lithium ion concentration in the liquid can be approximated to steady-state [30,33]. Since the grid scale system here will be operating at low C-rates, we can assume constant values in the liquid phase. Additionally, using parabolic approximations and the volume average approach outlined by Subramanian et al., we can further increase the computational efficiency of the model [34,35]. Again, this approach is only valid at low rates and long times, which are both present in the systems tested for this paper. While MG systems contains large battery capacities, these battery packs can be made up of many individual cells in series and parallel configurations to account for the large capacities and required voltages of the system. Large capacity packs

have utilized both large format cells and small standard 18650 cells to create the required capacities. For large format cells with thick electrodes the electrolyte gradient through the electrode becomes more prevalent, reducing the validity of the SPM assumptions [36]. For the battery systems studied here, we assume that the thickness of the electrode does not invalidate the assumption that electrolyte concentrations can be held constant. The largest challenge to estimating SOC for an entire battery pack is the individual cell SOC estimation [37]. We assume that the individual cells within the larger battery pack are evenly balanced and therefore representative of the larger pack states.

The SPM uses equations (3.2)–(3.3) to track lithium concentrations at the electrodes and solid phase potentials at the electrode and separator regions. The SOC of the battery is directly related to the lithium concentration at the cathode and anode (Eq (1.1)). By accurately estimating the lithium concentration, the SPM allows for a much more accurate measure of SOC during battery operation than look-up tables and empirical models that use only current or voltage as a proxy for SOC. In addition to more accurate SOC, the SPM increases accuracy of voltage and energy measured based on applied current.

The SPM has proven to be a more accurate model when compared to the ECM because its governing equations reflect the actual electrochemical processes occurring in the battery [38]. Electrochemically based models have been shown to achieve higher accuracy than their ECM counterparts, but ECM continue to be used for real-time battery management systems (BMS) due to their simplicity and robustness within microcontroller environments [39–43]. For non-BMS studies, electrochemical models such as the SPM are favored [31,33,44]. In some cases, enhanced ECM models have been applied by using the SPM theory to increase model accuracy [45,46]. A major challenge for ECMs is accurately measuring the SOC of the battery when charging rates are not constant. For solar charging when the current is constantly changing throughout the day and the rates of charging vary seasonally as well, ECMs are not well calibrated to accurately predict the SOC, voltage, or energy output during the entire simulation period because they are not valid outside of the operating conditions for which they are developed [47]. For a battery being charged through solar power and discharged based on grid demand, the operating conditions are constantly changing, creating the need for an accurate model that can better account for changing conditions. The SPM has shown to be more adaptive to changing operating conditions. While an accurate ECM using complex circuits can be used for a single case study, the model will not retain its accuracy as well as the SPM over the entire lifetime of the study because of the changing operating conditions.

We compared the SPM to a common ECM that uses a voltage proxy for SOC estimation. The ECM was based on a circuit containing an open circuit voltage source, a series resistance and an element with a parallel resistance and capacitor [48–51]. The circuit can be represented by the equations [52]:

$$\frac{dV_C}{dt} = \frac{-1}{R_C C_C} V_C + \frac{1}{C_C} i_{app} \tag{3.4}$$

$$V_b = V_{OC} - V_C - R_0 i_{app} \tag{3.5}$$

where V_b is the battery voltage, V_{OC} is the open circuit voltage, V_C is the capacitance voltage, R_0 is the ohmic resistance, C_C is the capacitance, R_C is the capacitor parallel resistance, and i_{app} is the applied current. The ECM was calibrated based on a 1C charge rate and set to match the capacity of the SPM model. For a single charge the percent difference between the ECM and SPM was 1.2% for the

voltage and 1.3% for the SOC throughout charging, underestimating values early in the cycle and overestimating values later. While the difference is acceptable for a single cycle, the error will accumulate when the models are used to track multiple cycles.

Additionally, changing the applied current from the original current creates error in the ECM. When studying a test case of the MG system (12 h day with 1 BCSC and 4 h demand of 2 MDMP starting at 6PM) the ECM found the system running at 87.5% Autonomy and 100% battery utilization. The SPM found autonomy of 89.0% and battery utilization of only 94%. A major discrepancy with the ECM is the inaccuracy of the calculated voltage-SOC relationship when the operating conditions are changed. Under the test case the ECM shows 100% SOC being reached before the normal voltage cut-off, which is a response from the empirical nature of the SOC estimation method.

While including more rigorous physics-based battery models (beyond the SPM) may be useful for simulating single cycles, the use of the SPM allows for simulation of a year's worth of system data on the order of minutes which cannot be matched by higher-order models [38]. The balance of efficiency with accurate SOC, voltage, and energy output estimation that the SPM offers allows for better analysis without heavily increasing computational time.

In the model environment, the battery and solar cell systems are combined through a series of controls that manipulate where the power is being delivered throughout the system. During periods of no demand, any available power from the solar cells will go directly to charging the battery. Once demand begins, power will be provided directly from the solar cells with any power amount above the level of demand continuing to go into battery charging. If power from the solar cells decreases below the desired level of demand, the battery will begin to discharge to make up the difference. The system is controlled through a series of modeled switches that can divert the power within the system to any component, with the primary goal of meeting demand levels. Simulations were

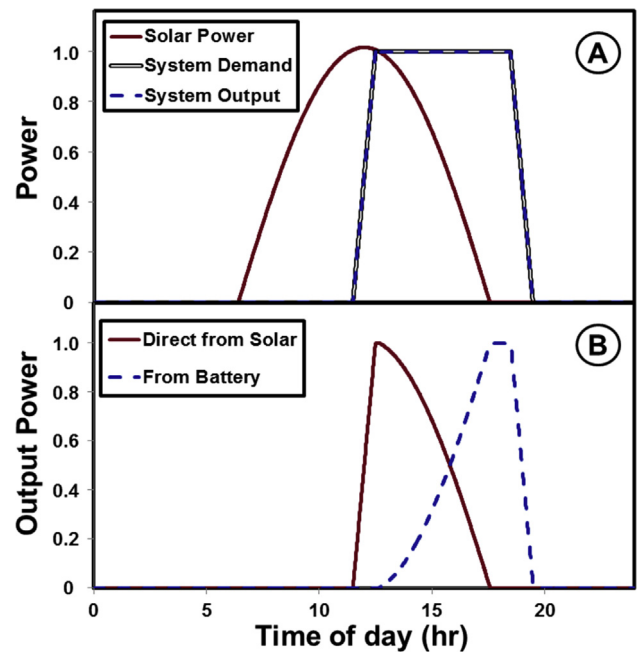


Fig. 2. Solar array plus battery storage with trapezoidal demand. A) Power from solar array is shown in conjunction with the demand of grid and the output of the system. B) Shows distribution of power that is supplied directly from solar array and power supplied from battery.

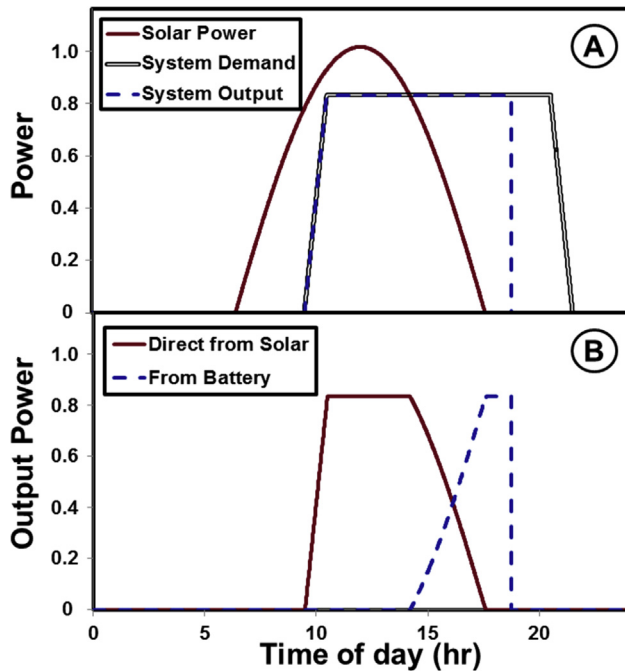


Fig. 3. Solar array plus battery storage with trapezoidal demand. In this case the system cannot meet demand at all times. A) Power from solar array is shown in conjunction with the demand of grid and the output of the system. B) Shows distribution of power that is supplied directly from solar array and power supplied from battery.

conducted in the MAPLESim environment and run with a variable-step Rosenbrock solver.

4. Single day case study

Two examples of the solar-battery system are shown in Figs. 2 and 3 to help explain the dynamic relationship between demand, generation, and storage. For the first case, a 12 h half sinusoidal solar insolation curve with peak solar insolation of 1000 W m^{-2} is used. The demand for the system is an 8 h trapezoid with a MDMP of 1 centered at 3:30PM (the trapezoid contains one hour of rising power demand, beginning at 11:30AM, and one hour of falling power demand ending at 7:30PM with a 6 h period of maximum demand in between). Fig. 2 shows that the power used directly from the solar array and from the battery storage meets demand at all times.

Fig. 3 shows a case where the energy demand is too great for the system under its current size and insolation. For a 12 h trapezoidal demand with a MDMP of 0.83 centered at 3:30PM, the solar array (same characteristics as previous case) does not produce enough energy and therefore supplies power only part of the time. In this case the system does not meet the required demand for 11.5% of the time, the system can only provide 79.4% of the demanded energy (Autonomy of 79.4%). Also important to note in the second case is that the capacity of the battery is underutilized, never being close to fully charged. Under the second case's conditions, the battery is only utilizing 57.2% of its total capacity during a single cycle (compared to 82.3% in case 1). The SOC is shown in Fig. 4 for both cases, showing how a fully charged battery state was never achieved. The SOC values here are calculated based on actual lithium concentration in the electrode, rather than as a proxy from voltage. The ability to track SOC based on internal parameters increase the accuracy of the measurement. In order to satisfy the external demand, the solar array's output must be increased (increasing the

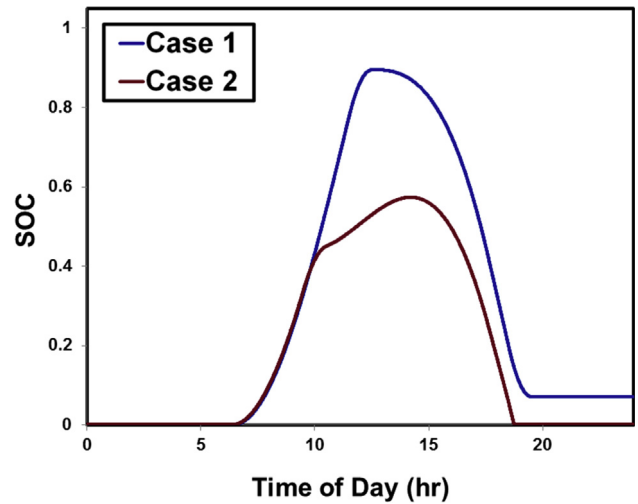


Fig. 4. SOC for cases in Figs. 3 and 4.

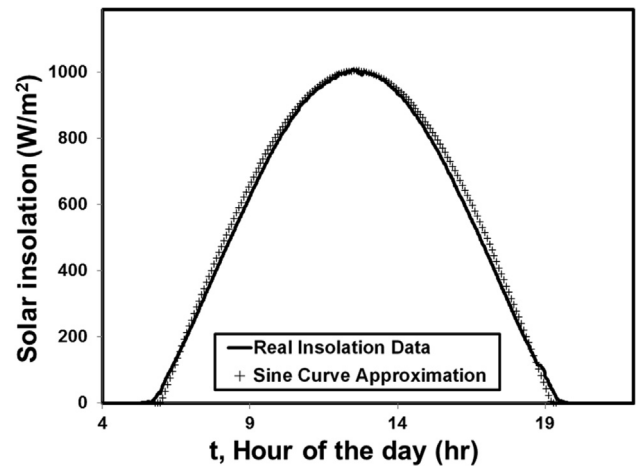


Fig. 5. Sinusoidal approximation versus real data from Phoenix site July 18th, 2012 [59].

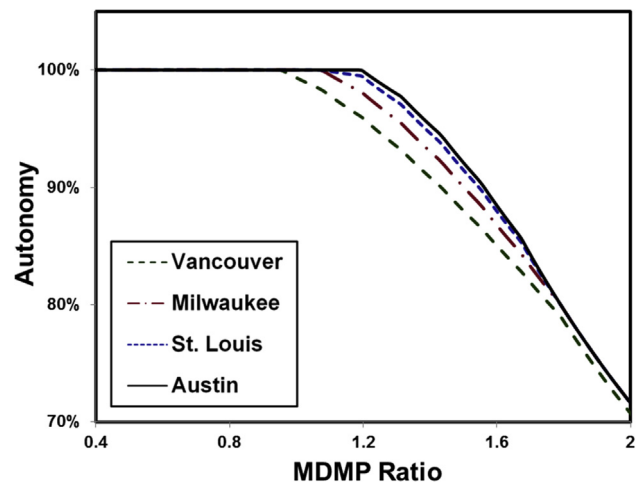


Fig. 6. Differences in yearly autonomy for four metropolitan regions based on the differences in day length variation based on latitude (weather indifferent) (BCSC 0.5).

array size 26% while keeping the rest of system constant) or the power demand decreased (decreasing the power demand by 21% while keeping the rest of the system constant).

5. Results

5.1. Influence of solar intermittency

For the study, half sine curves were used to approximate daily solar insolation curves. For completely sunny days, the half sinusoidal approximation compares well with actual solar insolation data. Fig. 5 shows our approximation compared to actual data for a day from Phoenix, AZ. However, our results will show an overestimate of available solar energy because we assume no daily deviations from the approximated curve.

To study annual averages to autonomy and utilization, we tested each case with insolation curves that ranged from 8 h of sunlight to 16 h of sunlight and weighted the values for how often that type of day length occurs during the year. An eight hour variation similar to the one in our study would be experienced near the 49th parallel (around the western US and Canadian border in the northern hemisphere). Fig. 6 shows 4 different cities that experience different seasonal variation in day length. Vancouver's (49°N) longest day is 8 h longer than the shortest day and its sunniest month provides 3.83 times as much solar energy as its darkest month. In Milwaukee, WI (43°N), St. Louis, MO (38°N), and Austin, TX (30.2°N) day length varies by 6.4 h, 5.5 h, and 4 h, respectively and the sunniest to darkest month energy ratio is 2.02, 1.89, and 1.66, respectively [25]. The effects of these variations on the autonomy of identical MG systems in each region are shown in Fig. 6.

5.2. Influences of demand variation

The trapezoidal and parabolic demands are more likely to be used by a grid-tied system and are representative of MG systems that wish to use their renewable energy to supplant the afternoon hours of peak demand. Both of these two types of demand were studied for demand periods ranging between 4 and 10 h.

The constant demand represents a system with a steady load requirement. The power demand will stay the same for the entire 24 h period. The sinusoidal demand also covers a 24 h period, but the amount of power demanded varies sinusoidally, peaking in midafternoon and being weakest overnight. For the sinusoidal

demand, the minimum power demand corresponds to half of the maximum power demanded. This demand structure is more representative of typical load curves for large MG and regional or national grids, which can see demand shift by over 100% during the course of a single day [53]. In general, the times of greatest solar insolation are weakly coincident with times of peak power demand. The lowest levels of power demand are during the nighttime and increase in early morning, reaching its peak in mid-afternoon, slightly after peak solar insolation (Often the peak demand will be ambient-temperature driven with high associated heating or cooling loads) [14,54,55].

5.3. Autonomy and utilization results

A system with no energy storage component can only meet demand when the solar insolation is greater than the required demand. The yearly autonomy for a system with no storage and a constant demand is shown in Fig. 7 as a function of power demand (in terms of MDMP ratio). Including storage within the system will increase the autonomy, but the energy capacity of the battery will determine how much the autonomy changes. Fig. 8 shows autonomy and battery utilization for three different battery sizes (BCSC-0.25, 0.5, and 1) under sinusoidal demand. As battery capacity increases, autonomy will increase, but only to the point where the power demanded exceeds the combined capacity of the solar array and battery. At this point, autonomy will remain the same (same in the BCSC 0.5 and 1 cases), while the battery utilization will begin to decrease because the battery can never be fully charged by the solar array. Table 2 shows the differences in battery utilization for differing demand and battery sizes.

The shape of MG demand affects the autonomy and battery utilization. Fig. 9 shows the autonomy and battery utilization for the four different types of demand curves with the MDMP Ratio normalized on an energy supplied basis (the same amount of energy is demanded by all 4 demand types at each MDMP Ratio) to allow for comparison of demand shape only. A MG that switches its demand from a sinusoidal demand to a trapezoidal demanded will experience greater autonomy, but lower battery utilization. The 24 h demand periods experience lower levels of autonomy because the percentage of energy demanded that is coincident with solar power is lower than the other cases.

In addition to the demand shape, for the parabolic and trapezoidal demands the timing of the demand load effects MG

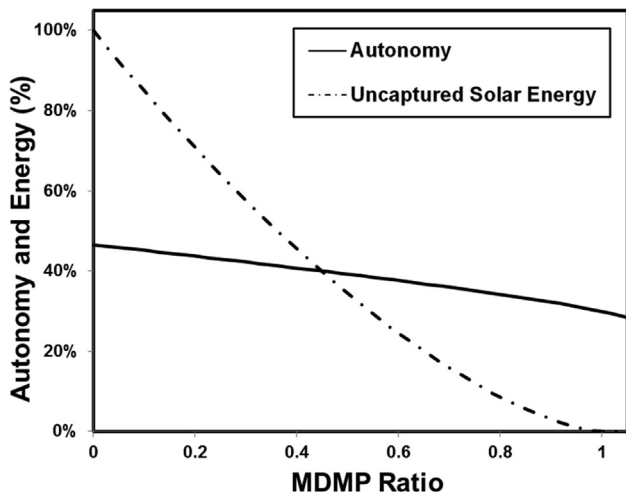


Fig. 7. Autonomy and uncaptured solar energy for solar array with no storage and constant demand.

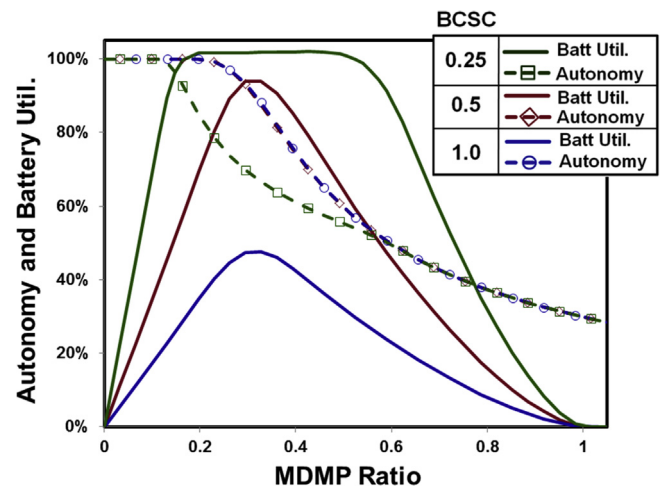


Fig. 8. Autonomy and battery utilization of sinusoidal demand for different battery sizes.

Table 2
Battery Utilization for the maximum power output demanded that still yields 100% autonomy for each of the four types of demand under three different battery sizes.

| BCSC | Constant (%) | Sine (%) | 4 h Trap (%) | Parabolic 4 h (%) |
|------|--------------|----------|--------------|-------------------|
| 1.0 | 34.7 | 39.48 | 38.41 | 29.83 |
| 0.5 | 69.4 | 79.15 | 76.4 | 56.36 |
| 0.25 | 79.2 | 25.07 | 52.69 | 58.67 |

operation. Fig. 10 shows the variation in autonomy and battery utilization for a 6 h trapezoidal demand centered at different times of a day. In Fig. 10, the demand is always a 6 h trapezoidal demand (varying in energy demanded based on MDMP), but the timing of the load changes. The 6 h trapezoidal demand curves are centered to occur at noon, 3:30PM, 6PM, or 9PM shown in the legend as the deviation of the load timing from noon (0, 3.5, 6, and 9 h). Since the solar insolation being used for this study is an approximation that is symmetrical, the results show the difference in the load timing between the center of the demand curve and the center of the solar insolation curve. The shape of autonomy and especially battery utilization was affected by the time of demand, with the battery utilization being more linear (as it approaches its maximum) for demands that are not coincident with solar insolation. The closer the timing of the load is to the timing of solar insolation, the less the battery must be used to supplement power, which leads to higher levels of autonomy and lower levels of battery utilization. When building isolated microgrids some loads will be dispatchable allowing them to be turned on or off at different times throughout the day. In general for isolated systems, placing loads coincident with available solar power will provide the greatest benefit.

Figs. 11–14 show cases that study the variation in demand length for the parabolic and trapezoidal demand curves being used for relieving peak loads. Three-dimensional plots of autonomy (Fig. 11) and battery utilization (Fig. 12) with a BCSC of 0.5 for all trapezoidal demand lengths are shown (Note a reversed x-axis (MDMP ratio) in Fig. 12 is used to show the main contour of the battery utilization plot in three dimensions). For the case shown in Figs. 11 and 12, when the 4 h trapezoidal demand is required, the battery storage capacity of BCSC 0.5 is well sized between MDMP of 1.5 and 2. However, when the 10 h trapezoidal demand is required, the battery storage is poorly sized, never reaching over 60% of utilization.

Similar effects are present in the case of parabolic demand curves. Three dimensional plots of autonomy (Fig. 13) and battery utilization (Fig. 14) for all parabolic demand lengths are shown (Note a reversed x-axis (MDMP ratio) in Fig. 14 is used to show the main contour of the battery utilization plot in three dimensions). The major difference between the trapezoid and parabolic demand is that the parabolic demand is thinner than the equivalent trapezoid demand resulting in slightly higher levels of autonomy and battery utilization shown in Figs. 13–14.

6. Discussion

When determining the best possible size and use of a solar battery system within a MG, many individual factors about the site and desired uses within the MG environment must be taken into account. No single solution will fit all the cases. The study for this paper offers an outline of how to approach best determining a system's size and operational characteristics by establishing the model for determining the relationship between a system's autonomy and the battery utilization associated with different applications. Autonomy and battery utilization cannot be maximized simultaneously in most cases. Rather a balance which best fits the consumer's needs and the site must be reached between both

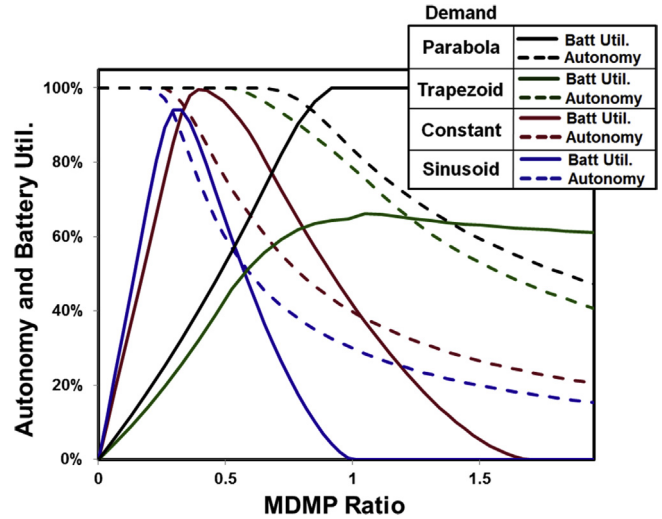


Fig. 9. Autonomy and battery utilization of each of the four demand types under the same sized system (BCSC 0.5).

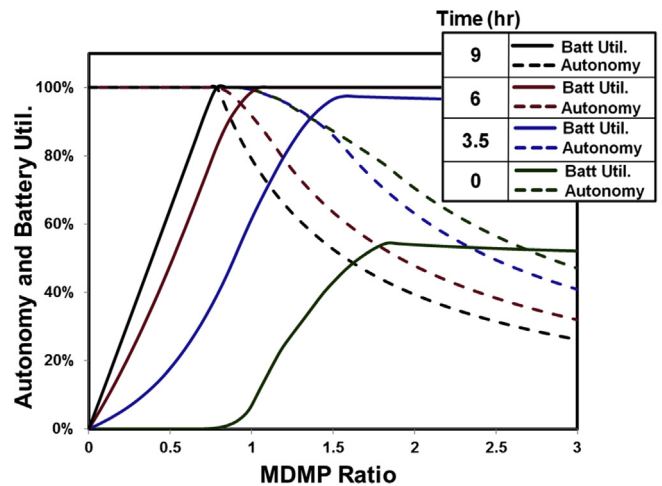


Fig. 10. Autonomy and battery utilization based on timing of trapezoidal demand. The time represents the trapezoid's variation from maximum solar insolation.

metrics. Using the methods outlined in this paper, future work will begin to focus on individual sites using site insolation and weather patterns to help determine best case system and operational characteristics for MG objectives.

One assumption of the paper is that increased battery utilization is always beneficial in the lifetime effectiveness of a battery system. Changes in DOD will affect the cycle life of a battery [56]. The relationship between DOD and cycle life is not well understood, however some cases have shown that lower levels of DOD can increase the nominal cycle life of the battery when accounting for lifetime energy storage [57,58]. Operating a battery at lower DOD will increase the cycle life, but will require a larger initial battery capacity and therefore higher upfront cost. Assuming a linear increase in nominal cycle life with a decrease in DOD, in order to see any economic benefit from installing a larger capacity battery and operating at lower DOD, the increase in nominal cycle life would need to increase at a rate of at least one percentage point for every percentage point decrease in DOD. Fig. 15 shows the relationship of system cost in respect to average DOD and rate of nominal cycle life increase. The nominal cycle life slope is a measure of how much the battery's nominal cycle life will increase due to lowered DOD. At a

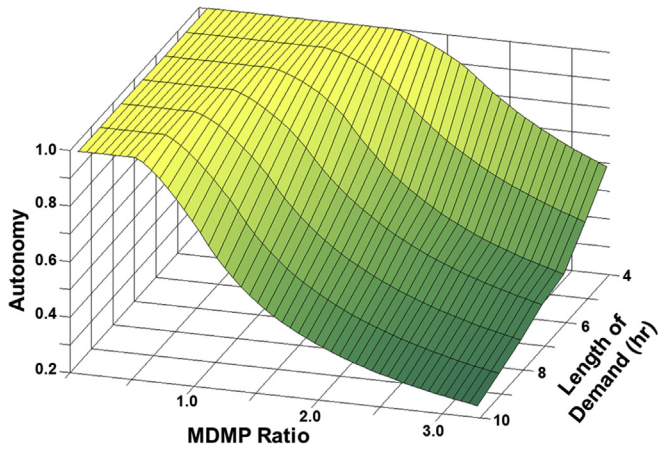


Fig. 11. Autonomy for all trapezoidal demand lengths (BCSC 0.5).

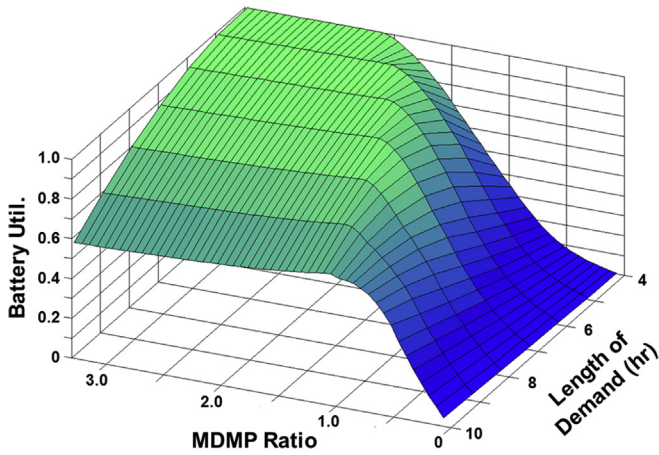


Fig. 12. Battery utilization for all trapezoidal demand lengths (BCSC 0.5). Note that the x-axis (MDMP ratio) has been inverted in order to highlight the contours.

slope of one, there would be no gain in nominal lifetime. The battery would output the same amount of energy over its lifetime (For example: 1000 cycles at 100% DOD or 2000 cycles at 50% DOD). For any slope greater than one, the total energy the battery can discharge during its lifetime will be greater at lower DOD. The slope is a relative measure of how much additional energy output can be

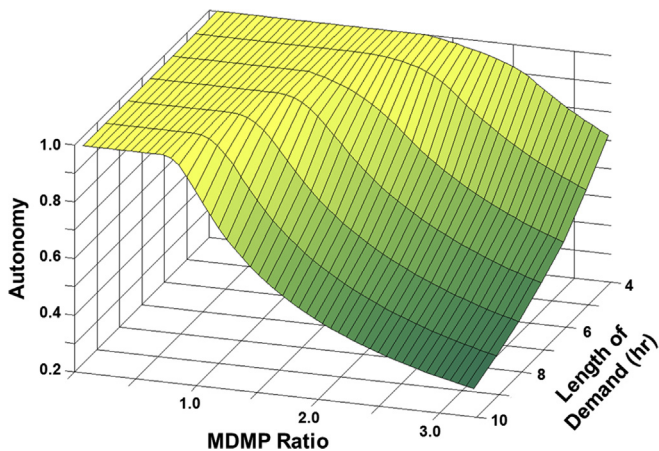


Fig. 13. Autonomy for all parabolic demand lengths (BCSC 0.5).

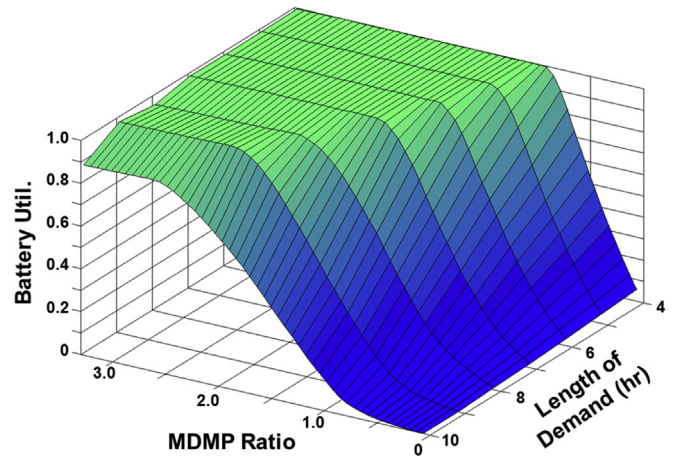


Fig. 14. Battery utilization for all parabolic demand lengths (BCSC 0.5). Note that the x-axis (MDMP ratio) has been inverted in order to highlight the contours.

gained from operating at a lower DOD. However, these increases can be partially offset by the need for a larger initial battery. The normalized lifetime cost measured in Fig. 15, accounts for both the increase in battery lifetime from the nominal cycle life slope and the increased initial battery capacity needed to operate at lower DOD and is normalized to the cost per kWh supplied (over the entire lifetime) for a battery operating at 100% DOD.

$$\text{Lifetime Cost} = \frac{\text{Initial Battery Cost}}{\text{Total Energy Provided}} \tag{6.1}$$

While small gains in lifetime cost can be seen at small DOD reductions and low nominal cycle life slopes, the types of nominal cycle life increases required to see economic benefits are greater than those from experimental studies for Li-ion batteries and therefore attempting to achieve the highest battery utilization is beneficial for system economics [56–58].

7. Conclusions

During the course of the year, the variation in solar insolation and demand makes it difficult to determine the best MG system components for meeting specific demand requirements. Consumers often have to choose between maximizing autonomy or

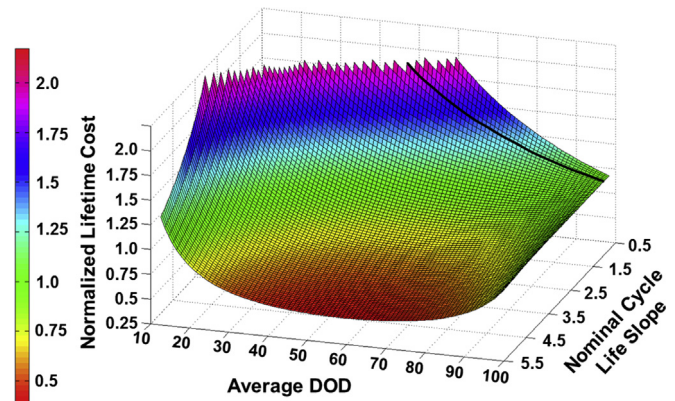


Fig. 15. Normalized battery lifetime cost as a function of average DOD and increase in nominal life due to shallower DOD (shown as nominal cycle life slope). All costs are normalized to the cost of a 100% DOD system. The black line represents no change in nominal cycle life due to shallower DOD (Nominal Cycle Life Slope = 1). Assumes a linear approximation of nominal cycle life as a function of DOD.

battery utilization. This paper outlines a model for determining MG system autonomy and battery utilization based on application demand and system size. This model can be used to establish the best possible solar array and battery storage for a desired application. Under the demand types tested, we found that demand shape and timing affect the system autonomy and battery utilization. When studying autonomy, the solar array size had a greater effect, while the battery size had a greater effect on battery utilization.

Use of the SPM allowed for greater accuracy when studying the SOC, energy output, and battery utilization for batteries operating in conjunction with intermittent renewable generation when compared with empirical battery estimates. The model allowed for fast and accurate simulation of the combined systems and enhanced the system's ability to control energy storage while maintaining safety and performance.

As more MG and DER enter the grid, tighter control and monitoring of a regional network of grids will be important in fully utilizing the available power capacity. Future work will use real solar insolation patterns from regional sites along with true demand curves in order to better assess how individual systems will function and to determine how similar systems placed in different locations (experiencing differing solar insolation and weather patterns) will affect the system's autonomy and battery utilization. Additional future work will look to include fade mechanisms into the SPM for better lifetime assessment of systems. Knowledge of the internal states through the SPM allows for more accurate fade mechanisms to be included in the future.

List of abbreviations, variables, parameters, and units.

| Abbreviations | |
|---------------------------------------|---|
| MG | Microgrid |
| DER | Distributed Energy Resource |
| LPSP | Loss of Power Supply Probability |
| SOC | State of Charge |
| DOD | Depth of Discharge |
| MDMP | Max Power Demanded to Max Solar Output Ratio |
| BCSC | Battery Energy Capacity to Solar Energy Capacity Ratio |
| ECM | Equivalent Circuit Model |
| SPM | Single Particle Model |
| NREL | National Renewable Energy Laboratory |
| SWERA | Solar and Wind Resource Assessment |
| BMS | Battery Management System |
| Variables and parameters | |
| P_D | Power demanded |
| P_G | Power generated |
| c^s | Lithium concentration (solid phase) |
| c | Lithium ion concentration (liquid phase) |
| c_{\max}^s | Maximum lithium concentration for solid phase |
| D_s | Solid phase diffusion coefficient |
| SOC_{initial} | State-of-Charge at beginning of discharge |
| SOC_{final} | State-of-Charge at end of discharge |
| Battery Utilization _{Annual} | Annual Battery Utilization |
| Energy _{discharged} | Energy discharged during simulation |
| Energy _{100%DOD} | The amount of energy discharged for a single 100% DOD cycle |
| Capacity _{Storage} | Storage Capacity |
| j | Flux at electrode surface |
| k | Reaction rate constant |
| F | Faraday's constant |
| R | Universal gas constant |
| T | Temperature |
| U | Open circuit potential |
| Φ | Potential |
| I | Solar array current |
| I_{PV} | Photovoltaic current |
| I_0 | Saturation current |
| V | Solar array voltage |
| V_t | Thermal voltage |
| V_b | Battery voltage (ECM) |
| V_{OC} | Open circuit voltage (ECM) |
| V_C | Capacitance voltage (ECM) |

(continued)

| R_s | Equivalent series resistance |
|-----------|-------------------------------------|
| R_p | Equivalent parallel resistance |
| R_C | Capacitor parallel resistance (ECM) |
| R_0 | Ohmic resistance (ECM) |
| C_C | Capacitance (ECM) |
| a | Diode ideality constant |
| i_{app} | Applied current (ECM) |
| Units | |
| MW | Megawatts |
| MWh | Megawatt-hours |
| Wm^{-2} | Watts per meter squared |

Acknowledgments

This research is based upon work supported by the Solar Energy Research Institute for India and the U.S. (SERIUS) funded jointly by the U.S. Department of Energy subcontract DE AC36-08G028308 (Office of Science, Office of Basic Energy Sciences, and Energy Efficiency and Renewable Energy, Solar Energy Technology Program, with support from the Office of International Affairs) and the Government of India subcontract IUSSTF/JCERDC-SERIUS/2012 dated 22nd Nov. 2012.

References

- [1] H. Jiayi, J. Chuanwen, X. Rong, A review on distributed energy resources and microgrid, *Renew. Sust. Energy Rev.* 12 (2008) 2472–2483.
- [2] J.A. Wood, B.F. Wollenberg, *Power Generation, Operation and Control*, John Wiley & Sons, Inc., New York, 1996.
- [3] A.M. Gopstein, Energy storage & the grid—from characteristics to impact, *P IEEE* 100 (2012) 311–316.
- [4] B. Yang, Y. Makarov, J. Desteese, V. Viswanathan, P. Nyeng, B. McManus, J. Pease, On the use of energy storage technologies for regulation services in electric power systems with significant penetration of wind energy, in: 5th International Conference on the European Electricity Market, 2008, p. 6.
- [5] H.S. Chen, T.N. Cong, W. Yang, C.Q. Tan, Y.L. Li, Y.L. Ding, Progress in electrical energy storage system: A critical review, *Prog. Nat. Sci.* 19 (2009) 291–312.
- [6] R.M. Dell, D.A.J. Rand, Energy storage - a key technology for global energy sustainability, *J. Power Sources* 100 (2001) 2–17.
- [7] J.M. Guerrero, J.C. Vasquez, J. Matas, L.G. de Vicuna, M. Castilla, Hierarchical control of droop-controlled AC and DC microgrids—a general approach toward standardization, *IEEE T Ind. Electron.* 58 (2011) 158–172.
- [8] J.A.P. Lopes, C.L. Moreira, A.G. Madureira, Defining control strategies for microgrids islanded operation, *IEEE T Power Syst.* 21 (2006) 916–924.
- [9] N. Hatzigiorgiou, H. Asano, R. Iravani, C. Marnay, Microgrids, *IEEE Power Energy Mag.* 5 (2007) 78–94.
- [10] M.A. Pedrasa, T. Spooner, A survey of techniques used to control microgrid generation and storage during island operation, in: Proceedings of the Australian Universities Power Engineering Conference, 2006, p. 6.
- [11] C. Proterogeropoulos, B.J. Brinkworth, R.H. Marshall, Sizing and techno-economic optimization for hybrid solar photovoltaic wind power systems with battery storage, *Int. J. Energy Res.* 21 (1997) 465–479.
- [12] B. Borowy, Z. Salameh, Methodology for optimally sizing the combination of a battery bank and PV array in a wind/PV hybrid system – reply, *IEEE T Energy Convers* 11 (1996) 374–375.
- [13] C. Budischak, D. Sewell, H. Thomson, L. Mach, D.E. Veron, W. Kempton, Cost-minimized combinations of wind power, solar power and electrochemical storage, powering the grid up to 99.9% of the time (vol 225, pg 60, 2013), *J. Power Sources* 232 (2013) 402.
- [14] C.H. Lo, M.D. Anderson, Economic dispatch and optimal sizing of battery energy storage systems in utility load-leveling operations, *IEEE T Energy Convers* 14 (1999) 824–829.
- [15] T.K.A. Brekken, A. Yokochi, A. von Jouanne, Z.Z. Yen, H.M. Hapke, D.A. Halamay, Optimal energy storage sizing and control for wind power applications, *IEEE T Sustain Energy* 2 (2011) 69–77.
- [16] S. Teleke, M.E. Baran, A.Q. Huang, S. Bhattacharya, L. Anderson, Control strategies for battery energy storage for wind farm dispatching, *IEEE T Energy Convers* 24 (2009) 725–732.
- [17] W.X. Shen, Optimally sizing of solar array and battery in a standalone photovoltaic system in Malaysia, *Renew. Energy* 34 (2009) 348–352.
- [18] S. Teleke, M.E. Baran, S. Bhattacharya, A.Q. Huang, Rule-based control of battery energy storage for dispatching intermittent renewable sources, *IEEE T Sustain Energy* 1 (2010) 117–124.
- [19] H.X. Yang, L. Lu, W. Zhou, A novel optimization sizing model for hybrid solar-wind power generation system, *Sol. Energy* 81 (2007) 76–84.
- [20] R. Chedid, S. Rahman, Unit sizing and control of hybrid wind-solar power systems, *IEEE T Energy Convers* 12 (1997) 79–85.

- [21] H.S.V.S.K. Nouna, S. Doolla, Energy management in microgrids using demand response and distributed storage—A multiagent approach, *IEEE T Power Deliv.* 28 (2013) 939–947.
- [22] H.X. Yang, W. Zhou, L. Lu, Z.H. Fang, Optimal sizing method for stand-alone hybrid solar-wind system with LPSP technology by using genetic algorithm, *Sol. Energy* 82 (2008) 354–367.
- [23] G. Nottton, M. Muselli, A. Louche, Autonomous hybrid photovoltaic power plant using a back-up generator: a case study in a mediterranean island, *Renew. Energy* 7 (1996) 371–391.
- [24] G. Nottton, M. Muselli, P. Poggi, A. Louche, Autonomous photovoltaic systems: influences of some parameters on the sizing: simulation timestep, input and output power profile, *Renew. Energy* 7 (1996) 353–369.
- [25] National Renewable Energy Laboratory, *Solar and Wind Energy Resource Assessment*, 2014. http://maps.nrel.gov/swera?visible=swera_dni_nasa_lo_res&opacity=50&extent=-179.14,18.92,-65.57,71.41.
- [26] S.S. Zhang, The effect of the charging protocol on the cycle life of a Li-ion battery, *J. Power Sources* 161 (2006) 1385–1391.
- [27] W. Zhou, C.Z. Lou, Z.S. Li, L. Lu, H.X. Yang, Current status of research on optimum sizing of stand-alone hybrid solar-wind power generation systems, *Appl. Energy* 87 (2010) 380–389.
- [28] M.G. Villalva, J.R. Gazoli, E. Ruppert, Comprehensive approach to modeling and simulation of photovoltaic arrays, *IEEE T Power Electr.* 24 (2009) 1198–1208.
- [29] M. Doyle, T.F. Fuller, J. Newman, Modeling of galvanostatic charge and discharge of the lithium polymer insertion cell, *J. Electrochem. Soc.* 140 (1993) 1526–1533.
- [30] G. Ning, B.N. Popov, Cycle life modeling of lithium-ion batteries, *J. Electrochem. Soc.* 151 (2004) A1584–A1591.
- [31] G.G. Botte, V.R. Subramanian, R.E. White, Mathematical modeling of secondary lithium batteries, *Electrochim. Acta* 45 (2000) 2595–2609.
- [32] C.Y. Wang, W.B. Gu, B.Y. Liaw, Micro-macroscopic coupled modeling of batteries and fuel cells - I. Model development, *J. Electrochem. Soc.* 145 (1998) 3407–3417.
- [33] S. Santhanagopalan, Q.Z. Guo, P. Ramadass, R.E. White, Review of models for predicting the cycling performance of lithium ion batteries, *J. Power Sources* 156 (2006) 620–628.
- [34] V.R. Subramanian, V.D. Diwakar, D. Tapriyal, Efficient macro-micro scale coupled modeling of batteries, *J. Electrochem. Soc.* 152 (2005) A2002–A2008.
- [35] S.K. Rahimian, S. Rayman, R.E. White, Extension of physics-based single particle model for higher charge-discharge rates, *J. Power Sources* 224 (2013) 180–194.
- [36] M. Guo, G. Sikha, R.E. White, Single-particle model for a lithium-ion cell: thermal behavior, *J. Electrochem. Soc.* 158 (2011) A122–A132.
- [37] L.G. Lu, X.B. Han, J.Q. Li, J.F. Hua, M.G. Ouyang, A review on the key issues for lithium-ion battery management in electric vehicles, *J. Power Sources* 226 (2013) 272–288.
- [38] V. Ramadesigan, P.W.C. Northrop, S. De, S. Santhanagopalan, R.D. Braatz, V.R. Subramanian, Modeling and simulation of lithium-ion batteries from a systems engineering perspective, *J. Electrochem. Soc.* 159 (2012) R31–R45.
- [39] X.S. Hu, S.B. Li, H. Peng, A comparative study of equivalent circuit models for Li-ion batteries, *J. Power Sources* 198 (2012) 359–367.
- [40] H.W. He, R. Xiong, J.X. Fan, Evaluation of lithium-ion battery equivalent circuit models for state of charge estimation by an experimental approach, *Energies* 4 (2011) 582–598.
- [41] S. Cho, H. Jeong, C. Han, S. Jin, J.H. Lim, J. Oh, State-of-charge estimation for lithium-ion batteries under various operating conditions using an equivalent circuit model, *Comput. Chem. Eng.* 41 (2012) 1–9.
- [42] T. Kim, W. Qiao, A hybrid battery model capable of capturing dynamic circuit characteristics and nonlinear capacity effects, *IEEE T Energy Convers.* 26 (2011) 1172–1180.
- [43] T.K. Dong, A. Kirchev, F. Mattera, J. Kowal, Y. Bultel, Dynamic modeling of Li-ion batteries using an equivalent electrical circuit, *J. Electrochem. Soc.* 158 (2011) A326–A336.
- [44] P.M. Gomadam, J.W. Weidner, R.A. Dougal, R.E. White, Mathematical modeling of lithium-ion and nickel battery systems, *J. Power Sources* 110 (2002) 267–284.
- [45] M.G. Ouyang, G.M. Liu, L.G. Lu, J.Q. Li, X.B. Han, Enhancing the estimation accuracy in low state-of-charge area: a novel onboard battery model through surface state of charge determination, *J. Power Sources* 270 (2014) 221–237.
- [46] G. Liu, L. Lu, H. Fu, J. Hua, J. Li, M. Ouyang, Y. Wang, S. Xue, P. Chen, A comparative study of equivalent circuit models and enhanced equivalent circuit models of lithium-ion batteries with different model structures, in: Presented at the Transportation Electrification Asia-Pacific, 2014 IEEE Conference and Expo, Beijing, China, 2014.
- [47] P.W.C. Northrop, B. Suthar, V. Ramadesigan, S. Santhanagopalan, R.D. Braatz, V.R. Subramanian, Efficient simulation and reformulation of lithium-ion battery models for enabling electric transportation, *J. Electrochem. Soc.* 161 (2014) 9.
- [48] Y.H. Chiang, W.Y. Sean, J.C. Ke, Online estimation of internal resistance and open-circuit voltage of lithium-ion batteries in electric vehicles, *J. Power Sources* 196 (2011) 3921–3932.
- [49] M. Dubarry, B.Y. Liaw, M.S. Chen, S.S. Chyan, K.C. Han, W.T. Sie, S.H. Wu, Identifying battery aging mechanisms in large format Li ion cells, *J. Power Sources* 196 (2011) 3420–3425.
- [50] G.L. Plett, Extended Kalman filtering for battery management systems of LiPB-based HEV battery packs – Part 2. Modeling and identification, *J. Power Sources* 134 (2004) 262–276.
- [51] T. Huria, M. Ceraolo, J. Gazzarri, R. Jackey, High fidelity electrical model with thermal dependence for characterization and simulation of high power lithium battery cells, in: Presented at the IEEE International Electric Vehicle Conference, Greenville, SC, 2012.
- [52] A. Rahmoun, H. Biechl, Modelling of Li-ion batteries using equivalent circuit diagrams, *Prz. Elektrotechniczn* 88 (2012) 152–156.
- [53] A. Chambers, *Distributed Generation: a Nontechnical Guide*, PennWell, Tulsa, OK, 2001.
- [54] A.G. Tsikalakis, N.D. Hatziaziyriou, Operation of microgrids with demand side bidding and continuity of supply for critical loads, *Eur. T Electr. Power* 21 (2011) 1238–1254.
- [55] C.A. Hill, M.C. Such, D.M. Chen, J. Gonzalez, W.M. Grady, Battery energy storage for enabling integration of distributed solar power generation, *IEEE T Smart Grid* 3 (2012) 850–857.
- [56] C.J. Rydh, B.A. Sanden, Energy analysis of batteries in photovoltaic systems. Part I: performance and energy requirements, *Energ. Convers. Manage* 46 (2005) 1957–1979.
- [57] J.D. Dogger, B. Roossien, F.D.J. Nieuwenhout, Characterization of Li-ion batteries for intelligent management of distributed grid-connected storage, *IEEE T Energy Convers.* 26 (2011) 256–263.
- [58] J. Wang, P. Liu, J. Hicks-Garner, E. Sherman, S. Soukiazian, M. Verbrugge, H. Tataria, J. Musser, P. Finamore, Cycle-life model for graphite-LiFePO₄ cells, *J. Power Sources* 196 (2011) 3942–3948.
- [59] National Renewable Energy Laboratory, *Measurement and Instrumentation Data Center (NREL)*, 2014. <http://www.nrel.gov/mid/>.